

Supporting Information

Beaded fiber composites – stiffness and strength modeling

Israel Greenfeld^{*,‡}, Carol W. Rodricks[‡], XiaoMeng Sui, and H. Daniel Wagner^{*}

Department of Materials and Interfaces, Weizmann Institute of Science, Rehovot 76100, Israel

*Corresponding authors e-mail addresses: green_is@netvision.net.il (I. Greenfeld),
Daniel.Wagner@weizmann.ac.il (H.D. Wagner)

Contents:

- S1. Beads contour shape
- S2. Rationale for approximate solution of the stresses
- S3. Tensile stiffness (modulus) approximation
- S4. Stress concentrations induced by neighboring fibers

S1. Beads contour shape

The shape of a liquid drop deposited on a fiber is determined by the equilibrium between surface tension and pressure (Figure S1).

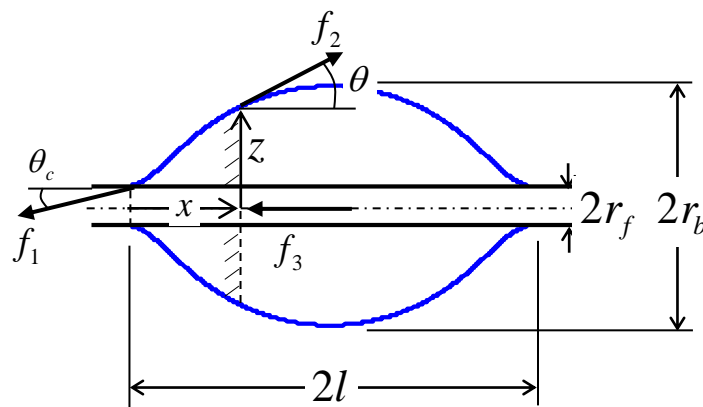


Figure S1. Shape of a liquid drop on a fiber. Forces acting on a drop segment (marked by dashed lines): f_1 and f_2 are forces due to surface tension, and f_3 is a force due to pressure difference.

The following differential equation, written with all length variables normalized for convenience by the fiber radius (setting $r_f = 1$), describes the drop geometry (de Gennes et al., 2004; Greenfeld et al., 2018)

$$\frac{z}{\sqrt{1+(dz/dx)^2}} - \frac{r_b - \cos\theta_c}{r_b^2 - 1} (z^2 - 1) = \cos\theta_c \quad (\text{S1})$$

Given r_b and θ_c , this equation can be integrated numerically from $z(0) = 1$ to $z(l) = r_b$. The profile of the right side of the drop is obtained by symmetry. Using the resulting bead half-length l , the volume of revolution of the drop is

$$v_b = 2\pi \int_0^l (z^2 - 1) dx \quad (\text{S2})$$

To obtain a beaded fiber, polymer drops can each be deposited individually, or created spontaneously by liquid coating. When a fiber is coated by a uniform liquid film, evenly spaced drops spontaneously form as a result of the Plateau-Rayleigh liquid instability phenomenon (de Gennes et al., 2004; Greenfeld et al., 2018). For coating radius r_0 , the distance between adjacent drops (or wavelength) is given by

$$\lambda = 2\sqrt{2}\pi r_0 \quad (\text{S3})$$

Assuming no volume loss during drops formation, the coating volume that fills up a single drop is

$$\pi(r_0^2 - 1)\lambda = 2\sqrt{2}\pi^2(r_0^2 - 1)r_0 \quad (\text{S4})$$

Equating this volume to that of equation (S2), and solving the cubic equation of r_0

$$r_0 = \frac{1}{3\alpha} + \alpha \quad (\text{S5})$$

$$\text{where } \alpha = \sqrt[3]{v + \sqrt{v^2 - 1/27}} \quad \text{and} \quad v = \frac{v_b}{4\sqrt{2}\pi^2}$$

So, given the drop-fiber contact angle and the drop peak radius, the beads shape and frequency are fully defined (Figure S2). The complete beads profile z along a multi-beaded fiber is then $z = 1$ in

fiber sections without beads, and $z = z(x)$ in section with beads, where x is the longitudinal position in the bead local coordinates.

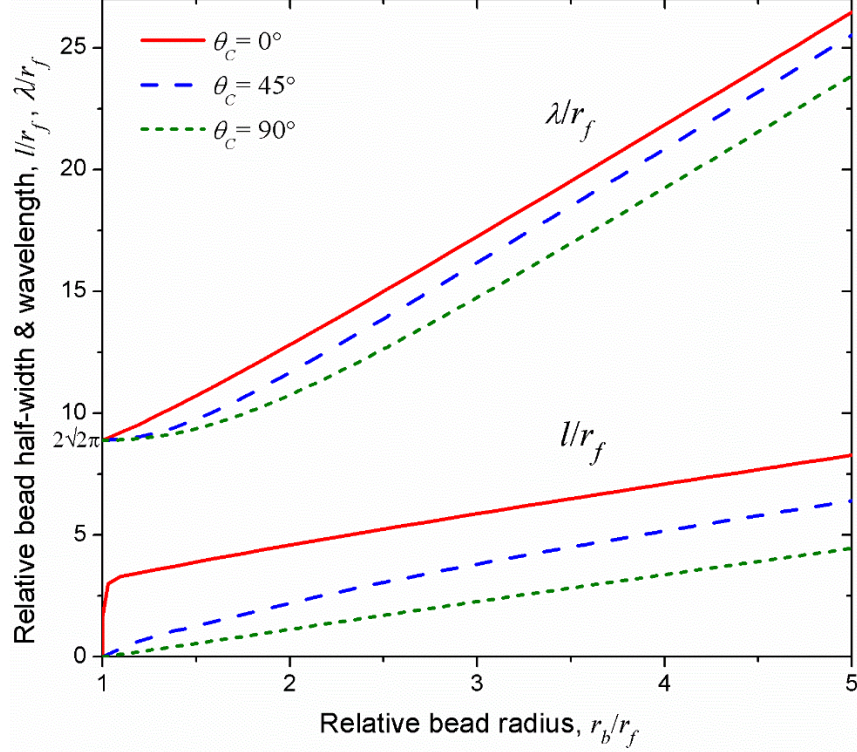


Figure S2. Bead shape parameters. Relative bead half-width l/r_f and beads wavelength λ/r_f vs. the bead relative radius r_b/r_f , for several bead-fiber contact angles θ_c .

S2. Rationale for approximate solution of the stresses

We seek an approximate solution for the differential equation of σ_f (equation (11)). The equation is rewritten with all length variables normalized for convenience by the fiber radius (setting $r_f = 1$)

$$\frac{d}{dx} \left(\frac{1}{n^2} \frac{d\sigma_f}{dx} \right) = \sigma_f - \varepsilon_1 E_f \quad (\text{S6})$$

where n is defined in equation (7) and its mean \bar{n} in equation (13). The bead profile, z , the local radius of the beads along the fiber, is an even periodic function of x with period λ (the distance between neighboring beads). Consequently, the dimensionless function n is also an even periodic

function of x with period λ . The examples of n normalized by \bar{n} in Figure S3 demonstrate that n can be described as a perturbation around \bar{n} . The perturbation amplitude grows with the beads size.

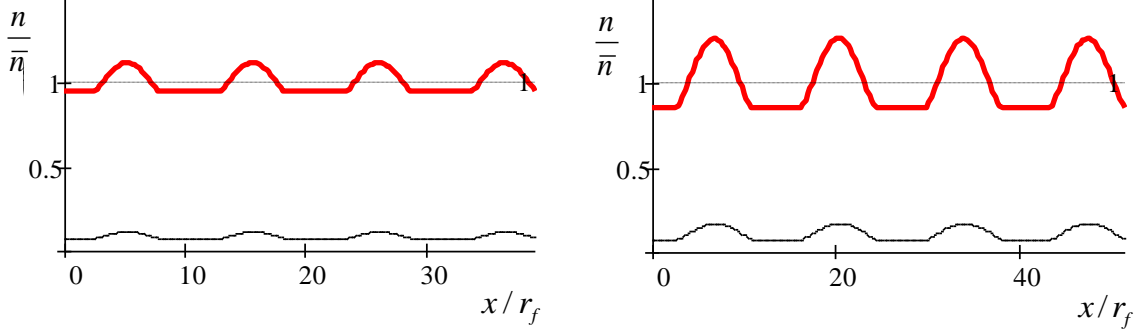


Figure S3. Examples of the function n . Normalized by the mean value \bar{n} . The beads profile is shown below for an 8-beaded fiber (only the right half is shown). The relative bead radius r_b/r_f is 1.5 for the left plot and 2.2 for the right plot, with volume fraction $V_f = 0.3$.

The particular solution of equation (S6) is $\sigma_f = \varepsilon_1 E_f$. The complementary solution of a linear differential equation with periodic coefficients was given by Floquet (Floquet, 1883), and is of the general form $\sigma_f = A\varphi(x)\sinh(\mu x) + B\psi(x)\cosh(\mu x)$, where A and B are constants to be derived from the boundary conditions, μ is a constant that depends on the coefficients of the Fourier series that represents the function n , and φ and ψ are even periodic functions of x with period λ . Given the boundary conditions $\sigma_f(-L) = \sigma_f(L) = 0$, we find $A = 0$ and $B = -\varepsilon_1 E_f / [\psi(L)\cosh(\mu L)]$. Thus, the solution for the fiber stress is of the form

$$\sigma_f = \varepsilon_1 E_f \left[1 - \frac{\cosh(\mu x) \psi(x)}{\cosh(\mu L) \psi(L)} \right] \quad (\text{S7})$$

Using equation (8), the solution for the shear stress is obtained by differentiating σ_f and is of the form

$$\tau_f = -\frac{1}{2} \frac{d\sigma_f}{dx} = \frac{1}{2} \mu \varepsilon_1 E_f \frac{\sinh(\mu x)}{\cosh(\mu L)} \frac{\varphi(x)}{\varphi(L)} \quad (\text{S8})$$

$$\text{where } \frac{\varphi(x)}{\varphi(L)} = \frac{\psi(x)}{\psi(L)} + \frac{d\psi(x)/dx}{\psi(L)} \frac{\coth(\mu x)}{\mu}$$

Rather than trying to determine φ and ψ explicitly, a difficult task given the implicit structure of the function n , itself a function of the implicit bead profile z , we resort to a perturbation approach comprising zero-order and first-order approximations.

The zero-order approximate solutions, given the boundary conditions $\sigma_f(-L) = \sigma_f(L) = 0$, were shown for the fiber tensile stress (equation (14))

$$\sigma_{f0} = \varepsilon_1 E_f \left[1 - \frac{\cosh(\bar{n}x)}{\cosh(\bar{n}L)} \right] \quad (\text{S9})$$

and for the fiber shear stress (equation (15))

$$\tau_{f0} = \frac{1}{2} \bar{n} \varepsilon_1 E_f \frac{\sinh(\bar{n}x)}{\cosh(\bar{n}L)} \quad (\text{S10})$$

However, these solutions do not reflect the stress fluctuations but just the mean stresses. Thus, we look for first-order approximations that would better describe the stress perturbations.

We start with τ_f , which incurs large perturbations (Figures 5 and 6) as a result of the fluctuations in n . To obtain the differential equation of τ_f , we differentiate equation (S6) and replace the derivative of σ_f by τ_f from equation (8)

$$\frac{d^2}{dx^2} \left(\frac{\tau_f}{n^2} \right) = \tau_f \quad (\text{S11})$$

We make the substitution $\hat{\tau}_f = \tau_f / n^2$ to arrive at the following differential equation

$$\frac{d^2 \hat{\tau}_f}{dx^2} = n^2 \hat{\tau}_f \quad (\text{S12})$$

The zero-order form of this equation is obtained by setting $n = \bar{n}$

$$\frac{d^2 \hat{\tau}_{f0}}{dx^2} = \bar{n}^2 \hat{\tau}_{f0} \quad (\text{S13})$$

and its solution, with the boundary condition $\hat{\tau}_f(0) = \tau_f(0) = 0$, is $\hat{\tau}_f = A \sinh(\bar{n}x)$, where A is a constant to be determined. Converting back to τ_f , we get the first-order approximation

$$\tau_{f\text{apx}} \cong n^2 \hat{\tau}_f \cong An^2 \sinh(\bar{n}x) \quad (\text{S14})$$

The mean (zero-order) stress is obtained by setting $n = \bar{n}$ in this equation, and therefore $\tau_{f0} \cong A\bar{n}^2 \sinh(\bar{n}x)$. Equating this result with τ_{f0} from equation (S10), we receive the constant $A = \varepsilon_1 E_f / [2\bar{n} \cosh(\bar{n}L)]$. Thus,

$$\tau_{f\text{apx}} \cong \frac{1}{2} \bar{n} \varepsilon_1 E_f \frac{\sinh(\bar{n}x)}{\cosh(\bar{n}L)} \frac{n^2}{\bar{n}^2} \quad (\text{S15})$$

This approximation restores the general Floquet solution shown in equation (S8), if the constant μ is substituted by \bar{n} and the function $\varphi(x)/\varphi(L)$ is replaced by n^2/\bar{n}^2 . Furthermore, the definition of the mean value $\bar{n} = \int_0^\lambda ndx/\lambda$ (equation (13)) constitutes the first coefficient in a Fourier series of n . Rearranging (using equation (S10)), we retrieve equation (16)

$$\tau_{f\text{apx}} \cong \tau_{f0} \frac{n^2}{\bar{n}^2} \cong \tau_{f0} + \tau_{f0} \left(\frac{n^2}{\bar{n}^2} - 1 \right) \quad (\text{S16})$$

where τ_{f0} is given in equation (S10). This first-order approximation comprises a mean reference component, τ_{f0} , and a perturbation component $\tau_{f0}(n^2/\bar{n}^2 - 1)$ that describes the periodic deviation from the mean.

The corresponding first-order solution for the fiber stress is obtained by integrating $\tau_{f\text{apx}}$ from the fiber end toward its center (using equation (8))

$$\sigma_{f\text{apx}} \cong -2 \int_L^x \tau_{f\text{apx}} dx \quad (\text{S17})$$

Using equation (S16)

$$\sigma_{f\text{apx}} \cong -2 \left[\int_L^x \tau_{f0} dx + \int_L^x \tau_{f0} \left(\frac{n^2}{\bar{n}^2} - 1 \right) dx \right] \quad (\text{S18})$$

The first integral yields the zero-order solution σ_{f0} , given in equation (S9), and finally equation (17) is retrieved

$$\sigma_{f\text{apx}} \cong \sigma_{f0} - 2 \int_L^x \tau_{f0} \left(\frac{n^2}{\bar{n}^2} - 1 \right) dx \quad (\text{S19})$$

This first-order approximation comprises a mean reference component, σ_{f0} , and a perturbation component that describe the periodic deviation from the mean. Integrating the second integral by parts

$$\sigma_{f\text{apx}} \cong \sigma_{f0} - 2 \left[\tau_{f0} \int_L^x \left(\frac{n^2}{\bar{n}^2} - 1 \right) dx - \int_L^x \frac{d\tau_{f0}}{dx} \int_L^x \left(\frac{n^2}{\bar{n}^2} - 1 \right) dx dx \right] \quad (\text{S20})$$

and neglecting the right-hand component, further simplification is achieved (at a small cost in accuracy)

$$\sigma_{f\text{apx}} \cong \sigma_{f0} - 2\tau_{f0} \int_L^x \left(\frac{n^2}{\bar{n}^2} - 1 \right) dx \quad (\text{S21})$$

The zero-order and first-order analytic approximations of the stresses in beaded fiber composites are exemplified in Figure S4 and compared to beadless fiber composites. Note that, at the fiber end and at its center, the first-order approximation for the fiber stress should coincide with the zero-order approximation, that is $\sigma_{f\text{apx}}(L) = \sigma_{f0}(L) = 0$ and $\sigma_{f\text{apx}}(0) = \sigma_{f0}(0) = \sigma_{f\text{max}}$. The reason for this is that there is no perturbation at the fiber center and at its end because $z(0) = z(L) = r_f$. Furthermore, the exact Floquet solution (equation (S7)) at these locations should coincide with the approximate solutions when supposing that $\mu = \bar{n}$. This leads to the following equality (using equation (S19))

$$\int_0^L \tau_{f0} \left(\frac{n^2}{\bar{n}^2} - 1 \right) dx = 0 \quad (\text{S22})$$

which enables accurate numeric derivation of \bar{n} .

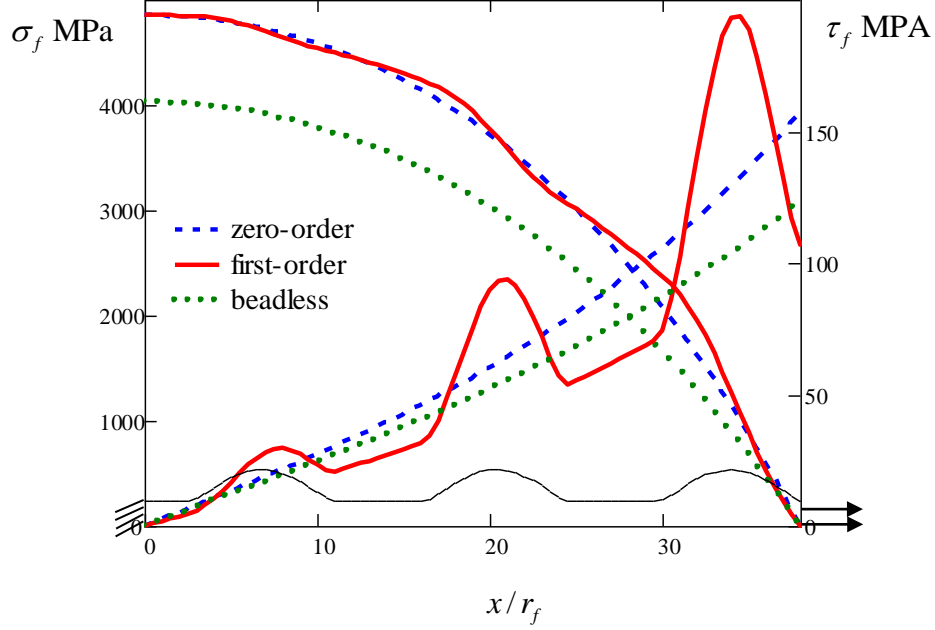


Figure S4. Analytic approximations of the stresses. The fiber tensile stress σ_f and interfacial stress τ_f , are depicted versus the relative position along the fiber, x/r_f , for beaded fibers with 6 beads (only the right half is shown) and for beadless fibers. The loading direction and symmetry plane are denoted. The composite strain is $\varepsilon_1 = 0.01$. The parameters are as in Figure 5.

S3. Tensile stiffness (modulus) approximation

We use the zero-order approximations to evaluate the composite stiffness (equation (25) in the main text). Executing the integration of equation (19) with σ_{f0} from equation (S9), the average fiber stress is

$$\bar{\sigma}_f \cong \frac{\varepsilon_1 E_f}{L} \int_0^L \left[1 - \frac{\cosh(\bar{n}x)}{\cosh(\bar{n}L)} \right] dx \cong \varepsilon_1 E_f \left(1 - \frac{\tanh(\bar{n}L)}{\bar{n}L} \right) \quad (\text{S23})$$

Similarly, to obtain the average bead stress we need to calculate the integral of equation (23), using σ_b from equation (22)

$$\bar{\sigma}_b \cong \frac{2\pi E_b}{\nu_b} \int_0^L \int_1^z \left[\frac{\sigma_f}{E_f} + \frac{\ln r}{G_b} \frac{d\tau_f}{dx} \right] r dr dx \quad (\text{S24})$$

remembering that ν_b is the cumulative volume of beads on half a fiber. Executing the inner integral

$$\bar{\sigma}_b \cong \frac{\pi E_b}{\nu_b} \int_0^L \left[(z^2 - 1) \frac{\sigma_f}{E_f} + \frac{z^2 \ln z}{G_b} \frac{d\tau_f}{dx} \right] dx \quad (\text{S25})$$

To enable an analytic solution of this integral, we simplify by defining a mean value for z , denoted \bar{z} , where $\nu_b = \pi(\bar{z}^2 - 1)L$, and substitute σ_{f0} from equation (S9) and τ_{f0} from equation (S10). The zero-order stress approximations are used rather than the first-order approximations, as the mean values should be adequate for evaluating the average stress. Executing the integration and rearranging

$$\bar{\sigma}_b \cong \varepsilon_1 E_b \left[1 - \frac{\tanh(\bar{n}L)}{\bar{n}L} K \right], \quad K = 1 - \frac{\bar{n}^2 \bar{z}^2 \ln \bar{z}}{2} \frac{E_f}{\bar{z}^2 - 1} \frac{1}{G_b} \quad (\text{S26})$$

Because the Plateau-Rayleigh beading generally maintains a constant ratio between the bead diameter and the wavelength (Greenfeld et al., 2018), a good initial guess for \bar{z} can be obtained by the average $\bar{z} \cong (r_b + 1)/2$. The range of the factor is $0 < K < 1$ for typical configurations, and it can be roughly estimated by $K \approx 1 - G_m / G_b$.

Substituting the results for $\bar{\sigma}_f$ and $\bar{\sigma}_b$ into the modulus equation (25) (in the main text)

$$E_{\text{lapx}} \cong V_f E_f \left[1 - \frac{\tanh(\bar{n}L)}{\bar{n}L} \right] + V_b E_b \left[1 - \frac{\tanh(\bar{n}L)}{\bar{n}L} K \right] + V_m E_m \quad (\text{S27})$$

The accuracy of this approximation is quite good, as exemplified in Figure S5. Fine tuning of \bar{n} can further improve the fitting accuracy. When $G_m / G_b \ll 1$, $K \approx 1$ and equation (S27) can be further simplified at the expense of a slightly lesser accuracy:

$$E_{\text{lapx}} \cong (V_f E_f + V_b E_b) \left[1 - \frac{\tanh(\bar{n}L)}{\bar{n}L} \right] + V_m E_m \quad (\text{S28})$$

Here, as well, fine tuning of \bar{n} can improve the fitting accuracy.

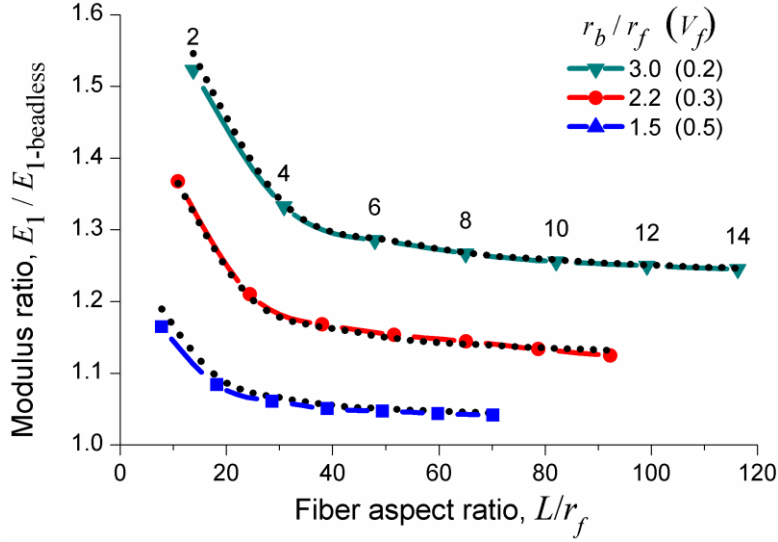


Figure S5. Accuracy of approximate composite modulus. The composite modulus E_1 , normalized by the modulus of a beadless fiber composite, is depicted versus the fiber aspect ratio, L/r_f , for several values of the relative bead radius r_b/r_f and corresponding maximal fiber volume fraction V_f . The solid lines are the numerical results at the same conditions as in Figure 10c. The dotted lines are the analytic approximations of equation (S27), without fine tuning of \bar{n} .

S4. Stress concentrations induced by neighboring fibers

The shear-lag elastic analysis assumes averaging of the composite stress and strain over a cross section through a large number of fibers. However, for the purpose of identifying the composite strength and failure mode, the calculation made in section 7 is approximate, as local stress concentrations in the bead, matrix and fiber induced by nearby fibers may change the ultimate stresses in these components. The following analysis provides a more accurate calculation of the local stresses based on the shear-lag approach, more specifically on the mechanism of load transfer from a broken fiber to a nearby intact fiber developed by (Eitan and Wagner, 1991; Wagner and Eitan, 1993) and further elaborated by (Grubb et al., 1995). This mechanism is adapted here to the equivalent configuration of load transfer from a nearby row of fibers to an affected fiber, where the longitudinal gap between two consecutive fibers in the row is analogous to a break in a long fiber (except for the minor effect of bonding at the fiber edge).

The beaded fiber in question is surrounded by several neighboring beaded fibers, whose number and distance is determined by the packing configuration/factor, P_f , and volume fraction, V_f , as described in section 2 and Figure 4. All the fibers are of the same length, $2L$, and carry the same number of beads. We start with a single row of nearby fibers (bright color in Figure S6a), which are offset by a distance l with respect to the affected fiber (dark color in Figure S6a). The shear stress at the surface of these fibers is $\tau_f(x')$, where $x' = x + l$ for the left fiber and $x' = x + l - 2L$ for the right fiber, and $\tau_f(x)$ is known from the analysis in sections 2 and 3. The tensile and shear stresses in the affected fiber and its neighbors, prior to load transfer, are shown in Figure S6b for an offset of $l = L/2$.

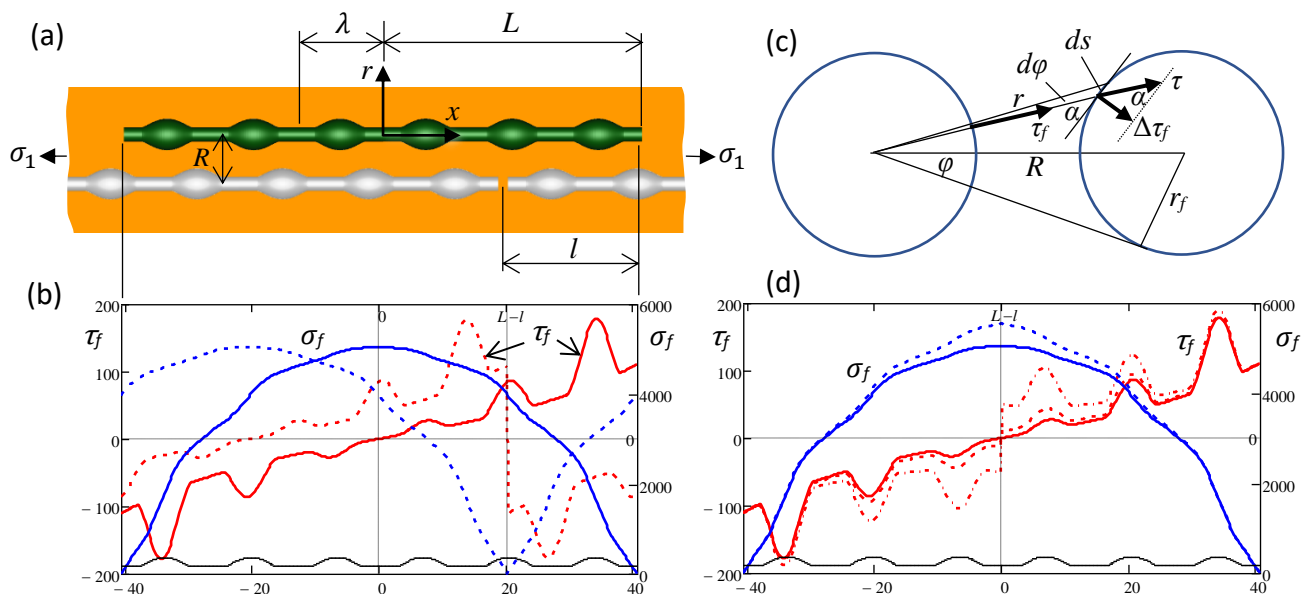


Figure S6. Stress transfer between neighboring fibers. (a) Affected fiber (dark color) and a row of nearby fibers (bright color) offset by l . (b) Fibers tensile and shear stresses prior to load transfer [MPa]: affected fiber (solid lines) and nearby fibers (dashed lines). The parameters are as in Figure S4. The offset is $l = L/2$. (c) Load transfer from nearby fiber (left) to affected fiber (right): geometry and shear stress vectors. (d) Tensile and shear stresses in the affected fiber [MPa] without load transfer (solid lines) and with load transfer (dashed lines); the max shear transfer is also shown (dash-dot line). The offset is $l = L$.

The load transfer model assumes that the shear stress at any longitudinal position x propagates radially from the fibers, and decays inversely proportional to the radial distance r (equation (3)):

$$\tau = \tau_f(x') \frac{r_f}{r} \quad (\text{S29})$$

This stress vector, shown at the surface of the affected fiber in Figure S6c, has a component that acts in the x direction, $\Delta\tau_f = \tau \sin(\alpha)$, on a surface segment $dsdx = rd\phi dx / \sin(\alpha)$. The total longitudinal force is obtained by integrating over the fiber face bounded by the $-\phi$ and ϕ tangent lines, $f = \int_{-\phi}^{\phi} \Delta\tau_f dsdx$, yielding $f = 2r_f \tau_f(x') \phi dx$. Dividing by the surface area of a circular ring, $2\pi r_f dx$, the average shear stress induced on the fiber is given by:

$$\Delta\tau_f(x) = -\tau_f(x') \frac{\phi}{\pi}, \quad x' = \begin{cases} x + l, & x \leq L - l \\ x + l - 2L, & x > L - l \end{cases} \quad (\text{S30})$$

Thus, the load transfer factor at any point along the x direction is ϕ/π . Note the negative sign which indicates that the longitudinal direction of the induced stress is opposite to that of the source stress. The angle ϕ can be written in terms of the packing factor and volume fraction (equation (1))

$$\phi = \sin^{-1}(r_f/R) = \sin^{-1} \sqrt{V_f/P_f} \quad (\text{S31})$$

Alternatively, ϕ may be defined by means of the intersections between effective interaction radii (Grubb et al., 1995), beyond which the stress perturbations in the matrix are negligible; this definition retains the load transfer concept but yields somewhat higher stress factors. The maximum $\Delta\tau_f$ occurs at the closest point between the fibers, where $r = R - r_f$ (equation (S29))

$$\Delta\tau_{f\max}(x) = -\tau_f(x') / \left(\sqrt{P_f/V_f} - 1 \right) \quad (\text{S32})$$

Finally, the change in the fiber stress due to $\Delta\tau_f$ is (equation (8))

$$\Delta\sigma_f(x) = -\frac{2}{r_f} \int_L^x \Delta\tau_f(x) dx = \frac{2\phi}{\pi r_f} \int_L^x \tau_f(x') dx \quad (\text{S33})$$

The total stresses with and without the load transfer effect are plotted in Figure S6d for an offset of $l = L$, showing a stress concentration peak in σ_f of magnitude $1 + \phi/\pi \cong 1.1$. A similar stress peak was observed by Raman stress concentration measurements by (Grubb et al., 1995). Also, the rise in the shear stress at its highest peak (at the position of the outermost beads) is ~ 1.06 when considering $\tau_{f\max}$. However, a more realistic representation of the load transfer should involve the load induced by all the nearby neighbors. For n close neighbors, arranged so that their offsets are

evenly spaced, that is $l = 2L/n$ and $l_i = il$ ($i = 0..n - 1$), the total load transfer obtained by equation (S30) is

$$\Delta\tau_f(x) = -\frac{\varphi}{\pi} \sum_{i=0}^{n-1} \tau_f(x'_i), \quad x'_i = \begin{cases} x + l_i, & x \leq L - l_i \\ x + l_i - 2L, & x > L - l_i \end{cases} \quad (\text{S34})$$

This is demonstrated in Figure S7a for square packing ($n = 4$). Note that $\Delta\tau_{f\max}$ is not presented in these plots because it is not cumulative, as the load transfer of each neighbor appears in a different angular section of the affected fiber. It is seen that the effect of load transfer from multiple nearby fibers tends to smoothen the stress concentrations, validating the basic shear-lag stress-averaging assumption noted at the beginning of this section. The cause for this smoothening is that the shear field induced by the fibers positioned with a smaller offset (close to non-staggered) assists the affected fiber (that is, reduces its load). This averaging effect will be enhanced if hexagonal packing would be used (6 fibers instead of 4), and if the load transfer from farther neighbors would be incorporated. Finally, when the longitudinal arrangement is not ordered, the offset positions may be arbitrary (Figure S7b), and some skewing of the stresses is observed, but the peak tensile and shear stresses in the affected fiber and its interface are not exceeded. Similar results were seen for higher stress concentration factors.

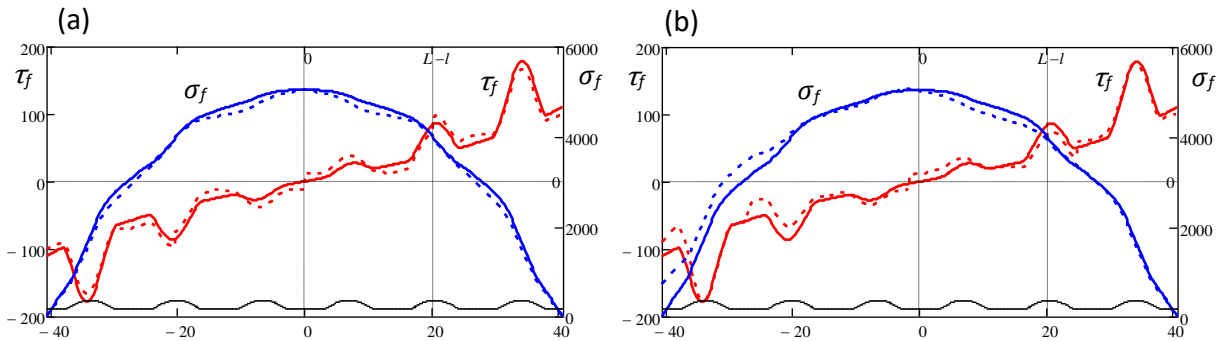


Figure S7. Cumulative stress transfer from 4 neighboring fibers. Affected fiber tensile and shear stresses [MPa], without load transfer (solid lines) and with load transfer (dashed lines). The parameters are as in Figure S4. The nominal offset is $l = L/2$. (a) The offset is $l_i = il$ ($i = 0..3$). (b) The offset is distributed uniformly over the range $l_i - l/2 \leq l_{i\text{rnd}} \leq l_i + l/2$.

References

- de Gennes, P.G., Brochard-Wyart, F., Quere, D., 2004. Capillarity and wetting phenomena - Drops, Bubbles, Pearls, Waves. Springer-Verlag New York, Inc.
- Eitan, A., Wagner, H.D., 1991. Fiber Interactions in 2-Dimensional Composites. *Appl. Phys. Lett.* 58, 1033-1035.
- Floquet, G., 1883. Sur les équations différentielles linéaires à coefficients périodiques. *Annales scientifiques de l'École Normale Supérieure Série 2: Volume 12*, 47-88.
- Greenfeld, I., Zhang, W., Sui, X., Wagner, H.D., 2018. Intermittent beading in fiber composites. *Composites Science and Technology* 160, 21-31.
- Grubb, D.T., Li, Z.F., Phoenix, S.L., 1995. Measurement of Stress-Concentration in a Fiber Adjacent to a Fiber Break in a Model Composite. *Composites Science and Technology* 54, 237-249.
- Wagner, H.D., Eitan, A., 1993. Stress-Concentration Factors in 2-Dimensional Composites - Effects of Material and Geometrical Parameters. *Composites Science and Technology* 46, 353-362.